liquids

MDPI

Article

Thermodynamics of Tetracycline Dissolution in Organic Solvents

Karen Michell Galindo-Delgado [1], Felipe Eduardo Andrade-Leiva [1], Jennifer Katiusca Castro-Camacho [2], Luis Daniel Ortega-Martínez [3], Fleming Martinez [4] and Daniel Ricardo Delgado [5,*]

1 Programa de Maestría en Ingeniería y Gestión Ambiental, Facultad de Ingeniería, Universidad Surcolombiana, Avenida Pastrana Borrero, Carrera 1, Neiva 410001, Colombia; u20261246680@usco.edu.co (K.M.G.-D.); u20261246611@usco.edu.co (F.E.A.-L.)
2 Hidroingeniería y Desarrollo Agropecuario, Programa de Ingeniería Agroindustrial, Facultad de Ingeniería, Universidad Surcolombiana, Neiva 410001, Colombia; jenniferkatiusca.castro@usco.edu.co
3 Facultad de Ingeniería Molecular y Tecnologías Sustentables, Decanato de Ingenierías, Universidad Popular Autónoma del Estado de Puebla, Calle 21 Sur 1103, Puebla 72410, Mexico; luisdaniel.ortega@upaep.mx
4 Grupo de Investigaciones Farmacéutico-Fisicoquímicas, Departamento de Farmacia, Facultad de Ciencias, Universidad Nacional de Colombia, Sede Bogotá, Carrera 30 No. 45-03, Bogotá 111221, Colombia; fmartinezr@unal.edu.co
5 Grupo de Investigación de Ingenierías UCC-Neiva, Programa de Ingeniería Civil, Facultad de Ingeniería, Universidad Cooperativa de Colombia, Sede Neiva, Neiva 410001, Colombia
* Correspondence: danielr.delgado@campusucc.edu.co; Tel.: +57-321-910-4471

Abstract

Tetracycline (TTC) is a broad-spectrum antibiotic that has become an emerging contaminant due to its widespread use in human and veterinary medicine. The limited physicochemical data on its solid–liquid equilibrium hinders the development of pharmaceutical formulations and the modeling of its environmental fate. This study aimed to perform a thermodynamic analysis of TTC solubility in ten pure organic solvents between 278.15 and 313.15 K. Solubility was quantified using UV/Vis spectrophotometry and the shaking-flask method. The solid phases at equilibrium were analyzed using FTIR spectroscopy. The apparent standard thermodynamic functions of the solution were calculated using the Gibbs–van't Hoff–Krug model. The effect of the solvent was evaluated using the KAT-LSER multiparametric model. The results showed that solubility increased with temperature in all studied solvents, reaching its maximum value in *N*,*N*-dimethylformamide ($x_2 = 0.0431$ at 313.15 K) and its minimum in cyclohexane ($x_2 = 0.00000161$ at 278.15 K), decreasing in alcohols as the aliphatic chain lengthens or becomes branched. We conclude that dissolution is an endothermic process ($\Delta_{soln}H^\circ > 0$), favored primarily by enthalpy in polar media, and governed by the dipolarity/polarizability (π^*) of the solvent.

Keywords: tetracycline; solubility; thermodynamics of solutions; organic solvents; KAT-LSER model; Gibbs–van't Hoff–Krug model

Check for updates

Academic Editor: Ariel A. Chialvo

Received: 30 September 2026
Revised: 22 October 2026
Accepted: 26 October 2026
Published: 28 October 2026

Copyright: © 2026 by the authors. Licensee MDPI, Basel, Switzerland. This article is an open access article distributed under the terms and conditions of the Creative Commons Attribution (CC BY) license.

1. Introduction

Tetracyclines are a family of antibiotics that are characterized by a linear core of four connected rings, known as the naphthacene system (Figure 1) [1–3]. Their primary mechanism of action is their ability to bind reversibly to the 30S subunit of bacterial ribosomes. This blocks the coupling of aminoacyl-tRNA (aa-tRNA), which prevents the elongation of the polypeptide chain during protein synthesis [1,3]. Since their discovery in the mid-20th century, these drugs have been overprescribed in human and veterinary medicine for prophylaxis and treatment of infections caused by Gram-positive and -negative bacteria, as well as by Rickettsia, Mycoplasma, Chlamydia, and various protozoa [4]. Tetracyclines

have evolved into three generations; The first generation consists of natural analogs, such as oxytetracycline, chlortetracycline, and tetracycline [5]. The second generation comprises semisynthetic derivatives, such as doxycycline and minocycline [6]. The third generation consists of synthetic molecules, such as tigecycline and eravacycline; these third-generation drugs have been designed to optimize bioavailability and overcome pharmacokinetic barriers [7] in addition to their conventional uses in treating dermatological and respiratory conditions, as well as in gastrointestinal eradication regimens, such as therapy against *Helicobacter pylori*. Some studies have highlighted their non-antibacterial properties. These properties include anti-inflammatory and immunomodulatory effects, as well as significant antineoplastic potential through altering the cell cycle, modulating autophagy, and inducing apoptosis in multiple cancer cell lines [1].

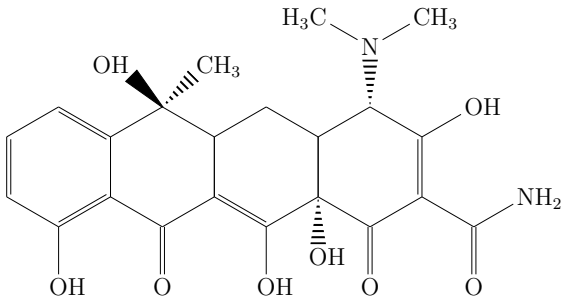


Figure 1. Molecular structure of Tetracyclinie (IUPAC Name: (4S,4aS,5aS,6S,12aS)-4-(Dimethylamino)-3,6,10,12,12a-pentahydroxy-6-methyl-1,11-dioxo-1,4,4a,5,5a,6,11,12a-octahydro-2-tetracenecarboximidic acid).

However, the clinical efficacy of tetracyclines is severely compromised by the emergence and widespread dissemination of antimicrobial resistance (AMR). This phenomenon is exacerbated by the intensive, prolonged, and often excessive use of tetracyclines in agricultural production and medical practice. The proliferation of multidrug-resistant strains has made antibiotic resistance one of the most significant global health problems [8,9].

According to the NORMAN network, this problem extends beyond hospital and community settings to environmental ecosystems, where tetracycline is classified as a highly persistent emerging contaminant [10]. Due to its limited metabolism in the gastrointestinal tract (between 30% and 90%), the ingested dose is excreted unchanged or in the form of bioactive metabolites through urine and feces [11]. The primary pathways for antibiotics to enter aquatic and edaphic systems are effluent discharges from wastewater treatment plants (WWTPs), whose conventional biological processes are largely ineffective at removing these molecules, along with agricultural runoff resulting from the use of contaminated manure as fertilizer and industrial pharmaceutical discharges [8,11,12]. In aquatic bodies and sediments, tetracycline strongly binds to organic matter, sediments, and microplastics. A dangerous consequence is that tetracycline becomes immobilized in biofilm matrices while retaining its bioavailability to benthic and sessile microbiota. This results in a continuous effect that stimulates the vertical and horizontal transfer of ARGs, altering native microbial diversity and inducing ecotoxic responses in phytoplankton, benthic invertebrates, and vertebrates, such as fish [11,13].

In this context, the pharmacological impact of tetracycline and its behavior in the environment are both governed by fundamental physicochemical processes [2,14]. As a highly polar and hydrophobic amphoteric molecule, solubility is one of its most important physicochemical properties, as it determines the partition of the drug between the different phases of the system [13,15]. From a biopharmaceutical standpoint, solubility is related to the rate of drug dissolution in the gastrointestinal tract [16]. In aquatic and edaphic

ecosystems, solubility controls tetracycline's mobility, regulating its dispersion in water, its tendency to chelate with divalent metal cations and its dynamic adsorption–desorption equilibrium with solid matrices such as activated sludge, sediments and microplastics [13]. Therefore, solubility determines not only the drug's antibacterial potency, but also the magnitude of its impact on the microbiota [13].

Given the complexity of these potential interactions, it is necessary to thermodynamically evaluate the drug dissolution process in order to generate data that will help elucidate the possible molecular mechanisms governing its behavior [14,17]. The standard apparent thermodynamic functions are determined using the Gibbs–van't Hoff–Krug model, which allows for the analysis of the energy contributions of the dissolution process [18,19]. This analysis of thermodynamic functions—enthalpy ($\Delta_{soln}H^{\circ}$), entropy ($\Delta_{soln}S^{\circ}$), and Gibbs energy ($\Delta_{soln}G^{\circ}$)—provides insight into possible molecular interactions between drugs and solvents. This information could be useful in developing more efficient industrial processes [20,21].

In order to analyze these interactions at a molecular level, the Kamlet–Abboud–Taft Linear Solvation Energy Relationship (KAT-LSER) model has become a key predictive tool for quantifying the impact of solvents and intermolecular forces on the solubility of nonelectrolytes. Thus, the KAT-LSER model provides an interpretation linking the structure of the solute to its solvation behavior in pure solvents [22–24]. Despite significant clinical, agronomic and ecological interest in tetracycline, systematic experimental data on solubility and temperature-dependent thermodynamic dissolution functions are lacking in the scientific literature. This lack of empirical information limits the accuracy of environmental transport models, hinders the optimization of pharmaceutical purification and crystallization processes, and often necessitates the use of unproven theoretical extrapolations. The primary rationale of this research is, therefore, to determine the equilibrium solubility of tetracycline through experimentation, characterize the thermodynamics of its dissolution and apply the KAT-LSER model to identify possible molecular interactions. This will generate a set of physicochemical data that can contribute to the design of effective therapeutic formulations, the modeling of the drug's environmental fate and the development of remediation technologies.

2. Materials and Methods

2.1. Reagents

In this study, Tetracycline (TTC) (Sigma-Aldrich, Burlington, MA, USA; compound **2**, *N*,*N*-dimethylformamide (DMF) (Sigma-Aldrich, Burlington, MA, USA; solvent component **1a**, purity of at least 0.998 in mass fraction), methanol (MeOH) (Sigma-Aldrich, Burlington, MA, USA; solvent component **1b**, purity of at least 0.9975 in mass fraction), ethanol (EtOH) (Sigma-Aldrich, Burlington, MA, USA; solvent component **1c**, purity of at least 0.995 in mass fraction), *n*-propanol (*n*-PrOH) (Supelco, Burlington, MA, USA; solvent component **1d**, purity of at least 0.995 in mass fraction), *i*-propanol (*i*-PrOH) (Supelco, Burlington, MA, USA; solvent component **1e**, purity of at least 0.995 in mass fraction), *n*-butanol (*n*-BtOH) (Sigma-Aldrich, Burlington, MA, USA; solvent component **1f**, purity of at least 0.999 in mass fraction), *n*-octanol (*n*-OcOH) (Sigma-Aldrich, Burlington, MA, USA; solvent component **1g**, purity of at least 0.998 in mass fraction), 1,4-dioxane (DX) (Panreac, Barcelona, MA, España; solvent component **1h**, purity of at least 0.995 in mass fraction), *n*-hexane (*n*-Hex) (Sigma-Aldrich, Burlington, MA, USA; solvent component **1i**, purity of at least 0.99 in mass fraction), cyclohexane (CHN) (Sigma-Aldrich, Burlington, MA, USA; solvent component **1j**, purity of at least 0.99 in mass fraction) (solvent component **1**), Sodium hydroxide (NaOH) (Sigma-Aldrich, Burlington, MA, USA, purity of at least 0.97 in mass fraction), and distilled water (W) with conductivity 2.0 < μS/cm were used.

2.2. Solubility Determination

Solubility was determined according to the flowchart shown in Figure 2 [25]; for phase separation, syringe filters with a pore size of 0.45 µm were used, IR analysis was performed using an infrared spectrometer MPA Bruker Optik GmbH (Karlsruhe, Alemania), and quantification was performed using an EMC-11-UV UV/VIS spectrophotometer (Dresden, Germany) (See Supplementary File).

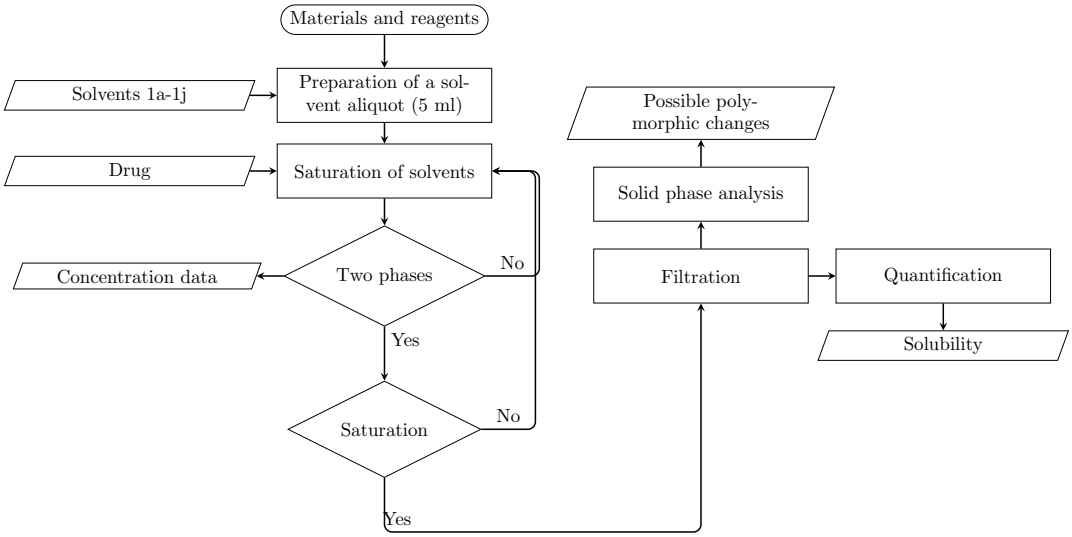


Figure 2. Flowchart of the experimental procedure for determining the solubility of drugs in cosolvent mixtures.

3. Results

Table 1 presents the experimental solubility data, which is expressed as a mole fraction. Thus, tetracycline (TTC) becomes more soluble in all the evaluated solvents as the temperature increases (Figure 3). As molecular mobility increases, the solute and solvent can interact to form new hydrogen bonds and dipole–dipole interactions, promoting the dispersion and dissolution of the drug. When analyzing the behavior of the series of linear alcohols (methanol, ethanol, *n*-propanol, *n*-butanol, and *n*-octanol), it is observed that solubility decreases as the aliphatic chain lengthens (greater number of carbon atoms). Thus, an increase in methylene groups ($-CH_2-$) enlarges the nonpolar region of the solvent molecule, favoring London dispersion forces between aliphatic chains while decreasing the relative density of the hydroxyl group. This could reduce the solvent's ability to form hydrogen bonds and dipole–dipole interactions with the multiple polar groups of TTC.

Caço et al. reported mole fraction solubilities of TTC in ethanol of 0.00613 at 288.15 K, 0.00732 at 293.15 K, and 0.0115 at 303.15 K [26]. When comparing these data with those obtained experimentally in this study, a relative discrepancy (calculated as $RPR = 100 \cdot (x_1 - x_2)/[(x_1 + x_2)/2]$ [27]) of 52.5% at 288.15 K, 47.5% at 293.15 K, and 49.32% at 303.15 K is observed. These discrepancies between laboratories are usually attributed to methodological factors (temperature control, experimental technique, and analytical method) or to the physicochemical characteristics of the solute (purity, polymorphic or enantiomeric forms). Upon reviewing the study by Caço et al., the only difference lies in the equilibration time; while Caço et al. report 6 h of equilibration, this study ensured a time of 36 h; a possible explanation is that the original solid used by Caço et al. contained an amorphous or microcrystalline phase, or a metastable polymorph with higher free energy, resulting in a transiently higher initial apparent solubility [28]. With prolonged equilibration times (36 h), the system typically undergoes secondary nucleation and conversion to

the thermodynamically more stable and less soluble polymorph; however, this remains mere speculation given the lack of solid-state analysis in both studies. At 6 h, the metastable polymorph had not yet reversed. In this regard, Jouyban points out that there is marked variability among laboratories in solubility measurements, even under seemingly identical conditions, which compromises the predictive power and fit of theoretical models [29]. In line with this, Vertzoni et al. point out that achieving true thermodynamic equilibrium in this type of system often requires times exceeding 24 h [30].

Table 1. Experimental solubility of TTC (2) in different organic solvents, expressed as mole fraction (x_2), at different temperatures. Average relative uncertainty in temperature is $u_r(T) = 0.05$ K. Experimental pressure $p = 0.097$ MPa.

Solvent	278.15 K	283.15 K	288.15 K	293.15 K	298.15 K	303.15 K	308.15 K	313.15 K
DMF	$2.08 \pm 0.02 \times 10^{-2}$	$2.33 \pm 0.02 \times 10^{-2}$	$2.61 \pm 0.03 \times 10^{-2}$	$2.90 \pm 0.03 \times 10^{-2}$	$3.22 \pm 0.03 \times 10^{-2}$	$3.55 \pm 0.03 \times 10^{-2}$	$3.91 \pm 0.03 \times 10^{-2}$	$4.31 \pm 0.03 \times 10^{-2}$
MeOH	$3.23 \pm 0.07 \times 10^{-3}$	$4.01 \pm 0.08 \times 10^{-3}$	$4.93 \pm 0.10 \times 10^{-3}$	$6.01 \pm 0.11 \times 10^{-3}$	$7.28 \pm 0.13 \times 10^{-3}$	$8.77 \pm 0.14 \times 10^{-3}$	$1.05 \pm 0.02 \times 10^{-2}$	$1.25 \pm 0.02 \times 10^{-2}$
EtOH	$2.22 \pm 0.05 \times 10^{-3}$	$2.83 \pm 0.07 \times 10^{-3}$	$3.58 \pm 0.08 \times 10^{-3}$	$4.51 \pm 0.09 \times 10^{-3}$	$5.62 \pm 0.11 \times 10^{-3}$	$6.95 \pm 0.13 \times 10^{-3}$	$8.54 \pm 0.15 \times 10^{-3}$	$1.04 \pm 0.02 \times 10^{-2}$
n-PrOH	$1.35 \pm 0.04 \times 10^{-3}$	$1.78 \pm 0.04 \times 10^{-3}$	$2.32 \pm 0.06 \times 10^{-3}$	$3.00 \pm 0.07 \times 10^{-3}$	$3.84 \pm 0.08 \times 10^{-3}$	$4.89 \pm 0.10 \times 10^{-3}$	$6.17 \pm 0.12 \times 10^{-3}$	$7.72 \pm 0.13 \times 10^{-3}$
i-PrOH	$5.93 \pm 0.18 \times 10^{-4}$	$8.17 \pm 0.24 \times 10^{-4}$	$1.11 \pm 0.03 \times 10^{-3}$	$1.50 \pm 0.04 \times 10^{-3}$	$2.00 \pm 0.05 \times 10^{-3}$	$2.65 \pm 0.06 \times 10^{-3}$	$3.47 \pm 0.07 \times 10^{-3}$	$4.52 \pm 0.09 \times 10^{-3}$
n-BtOH	$8.26 \pm 0.25 \times 10^{-4}$	$1.12 \pm 0.03 \times 10^{-3}$	$1.50 \pm 0.04 \times 10^{-3}$	$2.00 \pm 0.05 \times 10^{-3}$	$2.63 \pm 0.06 \times 10^{-3}$	$3.44 \pm 0.08 \times 10^{-3}$	$4.46 \pm 0.09 \times 10^{-3}$	$5.71 \pm 0.11 \times 10^{-3}$
n-OcOH	$2.96 \pm 0.10 \times 10^{-4}$	$4.18 \pm 0.14 \times 10^{-4}$	$5.82 \pm 0.18 \times 10^{-4}$	$8.01 \pm 0.24 \times 10^{-4}$	$1.09 \pm 0.03 \times 10^{-3}$	$1.47 \pm 0.04 \times 10^{-3}$	$1.97 \pm 0.05 \times 10^{-3}$	$2.60 \pm 0.06 \times 10^{-3}$
DX	$4.40 \pm 0.05 \times 10^{-4}$	$6.60 \pm 0.05 \times 10^{-4}$	$9.88 \pm 0.10 \times 10^{-4}$	$1.48 \pm 0.02 \times 10^{-3}$	$2.21 \pm 0.02 \times 10^{-3}$	$3.31 \pm 0.05 \times 10^{-3}$	$5.18 \pm 0.05 \times 10^{-3}$	$8.36 \pm 0.08 \times 10^{-3}$
n-Hex	$2.06 \pm 0.09 \times 10^{-6}$	$2.59 \pm 0.11 \times 10^{-6}$	$3.23 \pm 0.13 \times 10^{-6}$	$4.01 \pm 0.16 \times 10^{-6}$	$4.93 \pm 0.19 \times 10^{-6}$	$6.01 \pm 0.22 \times 10^{-6}$	$7.29 \pm 0.26 \times 10^{-6}$	$8.79 \pm 0.30 \times 10^{-6}$
CHN	$1.61 \pm 0.07 \times 10^{-6}$	$2.01 \pm 0.09 \times 10^{-6}$	$2.49 \pm 0.10 \times 10^{-6}$	$3.06 \pm 0.12 \times 10^{-6}$	$3.73 \pm 0.14 \times 10^{-6}$	$4.53 \pm 0.17 \times 10^{-6}$	$5.46 \pm 0.20 \times 10^{-6}$	$6.54 \pm 0.23 \times 10^{-6}$

When analyzing the solubility of TTC in alcohol isomers, it was observed that branching decreases solubility when comparing TTC's behavior in *n*-PrOH to its behavior in *i*-PrOH. The branching in *i*-PrOH creates a steric hindrance, making it difficult for the hydroxyl group to approach the bulky functional groups of TTC enough to form effective hydrogen bonds. In contrast, the linear structure of *n*-PrOH allows for better interaction. This behavior is also influenced by the nature of the solvent (see Figure 3). In amphiprotic solvents such as alcohols, TTC exhibits moderate to high solubility, primarily due to their ability to act simultaneously as proton donors and proton acceptors in the formation of hydrogen bonds, thereby establishing favorable specific interactions with the functional groups of TTC. In contrast, TTC exhibits low solubility in nonamphoteric solvents, such as *n*-Hex and CHN, because TTC relies on weak London dispersion forces, which are unable to break the TEC network. However, TTC exhibits the highest solubility in DMF, a polar aprotic solvent. DMF does not donate protons but exerts strong dipole–dipole forces and acts as a good hydrogen-bond acceptor for TTC.

When analyzing the solubility of TTC at 298.15 K as a function of the solvents' solubility parameter (δ_1), an increasing trend is observed as this value approaches the TTC solubility parameter ($\delta_2 = 37.37$ MPa$^{1/2}$; see Table 2 and Figure 4). The solubility of TTC in alkanes (*n*-Hex and CHN), which have solubility parameters close to 15 and 16 MPa$^{1/2}$ [31], is the lowest of all the results obtained in this study. In contrast, the solubility of TTC in alcohols exhibits a strict positive linear correlation; solubility increases proportionally from *n*-OcOH to methanol. However, DMF deviates from this trend because it has the highest solubility of all the solvents tested, with a solubility parameter of 24.80 MPa$^{1/2}$ [31]. This demonstrates that the specific intermolecular interactions in this system predominate over the general theoretical prediction of the solubility parameter.

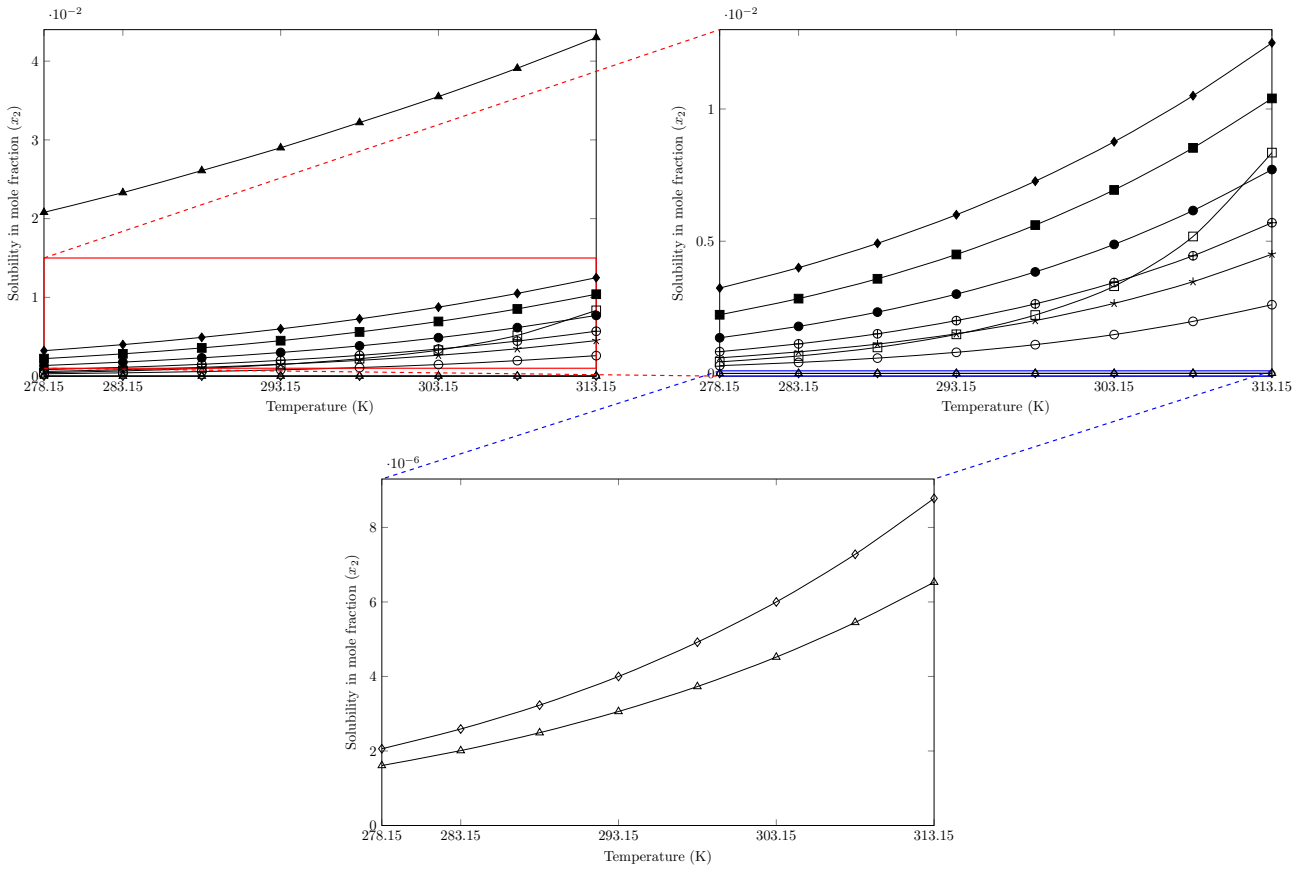


Figure 3. Solubility of TTC in different organic solvents (▲ = DMF, ♦: MeOH, ■: EtOH, ●: *n*-PrOH, ⋆: *i*-PrOH, ⊕: *n*-BtOH, ∘: *n*−OcOH, □: DX, ◇: *n*−Hex and △: CHN) at 8 temperatures (278.15 K to 313.15 K).

Table 2. Calculation of the Hildebrand parameter of TTC from group contributions [31].

Group	#	Single		Total	
		ΔU (J/mol)	V (cm^3/mol)	ΔU (J/mol)	V (cm^3/mol)
(−CH_3)	3	4.71	33.5	14.1	100.5
(−CH_2−)	1	4.94	16.1	4.9	16.1
(>CH−)	3	3.43	−1.0	10.3	−3.0
(>C<)	2	1.47	−19.2	2.9	−38.4
(>C=)	4	4.31	−5.5	17.2	−22.0
(−OH)	3	29.8	10.0	89.4	30.0
(−CO−)	2	17.4	10.8	34.8	21.6
(−N<)	1	4.2	−9.0	4.2	−9.0
(−$CONH_2$)	1	41.9	17.5	41.9	17.5
(−OH adjacent)	2	21.9	13.0	43.8	26.0
Phenyl trisubs	1	31.9	33.4	31.9	33.4
Ring closure-5	3	1.05	16.0	3.2	48.0
Conj ring	2	1.67	−2.2	3.3	−4.4
			$\sum$	302.0	216.3
			δ_2	37.37	MPa$^{1/2}$

3.1. Solid-State Analysis

To evaluate possible changes in the TTC molecule due to degradation and to identify potential structural changes indicative of polymorphism or solvation, we analyzed the solid phases at equilibrium in each sample by infrared spectroscopy (IR). The IR spectrum of the

pure, high-purity commercial sample was used to compare the results for each sample's solid phases at equilibrium with the saturated solutions. Figure 5 shows the Fourier transform infrared (FTIR) spectroscopic analysis, which allows for evaluation of the chemical integrity and structural stability of TTC following dissolution in various organic media. The analysis uses the spectrum of the high-purity commercial reference sample as a reference in the wavenumber range between 4500 cm^{-1} and 500 cm^{-1}.

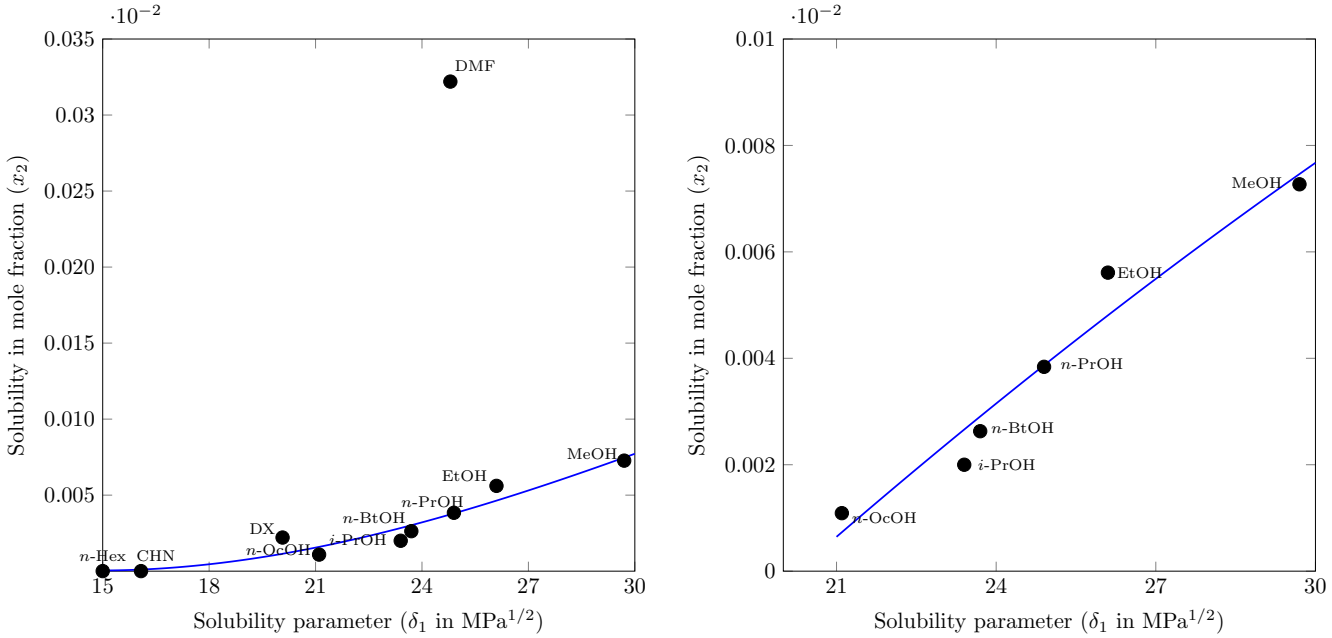


Figure 4. Correlation between the solubility of TTC at 298.15 K as a function of the solubility parameter of pure solvents.

When the transmittance profiles of the standard and solid phases recovered from solvents are compared, the positions of the wavenumbers and the morphologies of all absorption bands are found to correspond. In the high-frequency region between 3650 and 3200 cm^{-1}, all spectra exhibit the characteristic stretching signals of phenolic and alcoholic hydroxyl groups (O–H) and the stretching vibrations of the amide group (N–H) [32]. Between 3100 cm^{-1} and 2500 cm^{-1}, these signals are followed by a set of bands attributable to aromatic and aliphatic C–H stretching vibrations, along with intramolecular hydrogen-bonding interactions [32]. Between 1700 cm^{-1} and 1200 cm^{-1}, where the fundamental vibrations of the naphthacenocarboxamide skeleton are concentrated, including the stretching vibrations of the ketone (C=O) and amide carbonyl groups, as well as the stretching vibrations of the conjugated rings and the bending vibrations of the dimethylamino groups, no bathochromic or hypochromic shifts or peak splitting relative to the standard sample are observed.

Finally, the overlap observed in the fingerprint region—which lies between 1200 cm^{-1} and 500 cm^{-1}—allows us to rule out, with a high degree of confidence, the presence of additional bands associated with occluded residual solvent or the formation of stable solvates, as well as alterations in the crystal packing that might suggest polymorphic transitions. Therefore, the results of the eleven spectra indicate that TTC retains its molecular structure and original crystalline form, demonstrating that during the experimental equilibration and quantification process, the drug exhibits chemical and physical stability in the evaluated solvent systems.

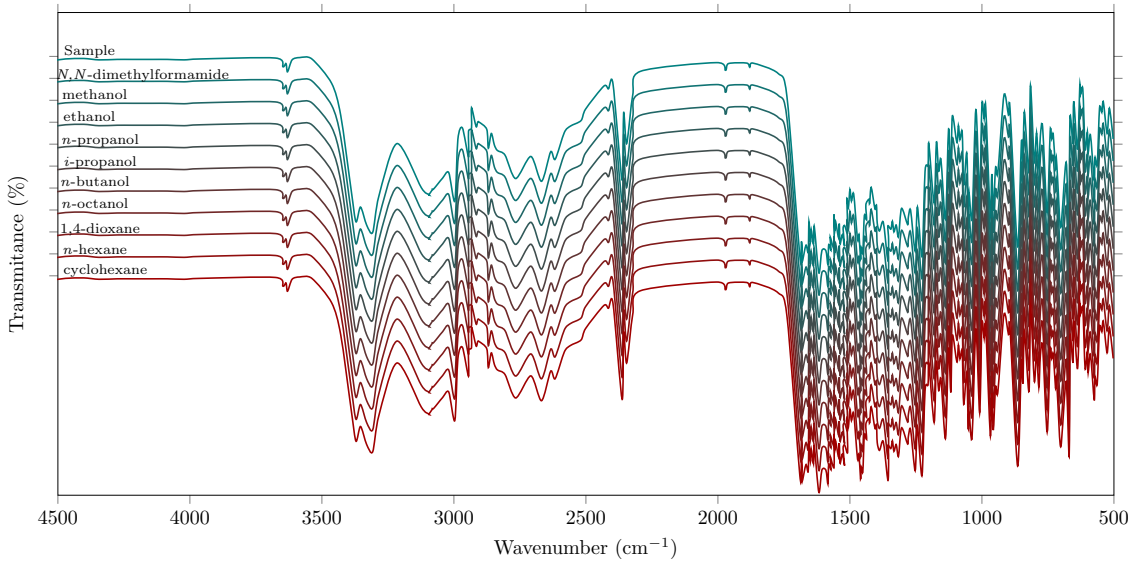


Figure 5. FTIR spectra of tetracycline in various pure solvents within the 4500–500 cm^{-1} region.

3.2. Thermodynamic Functions of Solution

The calculation of the thermodynamic functions for TCC dissolution based on experimental solubility data (Table 3) is based on van't Hoff's analysis, assuming a quasi-ideal dilute solution (where the solute activity coefficient tends to unity, $a_2 \approx x_2$), so the saturation equilibrium constant corresponds to the molar fraction of saturation (x_2). Thus, standard thermodynamic functions of dissolution take the infinitely dilute solution as the reference state for the solute ($\lim_{x_2 \to 0} \gamma_2 = 1$); in this state, each dissolved molecule is surrounded exclusively by solvent molecules and obeys Henry's law. Under this convention, the standard state of the solute in solution ($a_2^\circ = 1$) is a hypothetical state with a mole fraction of unity ($x_2^\circ = 1$), obtained via linear extrapolation from infinite dilution and in equilibrium with the pure crystalline solid ($a_{\text{solid}} = 1$). This allows the activity of the solute to be approximated by its mole fraction ($a_2 = \gamma_2 x_2 \approx x_2$) in dilute, saturated solutions. Consequently, the thermodynamic parameters derived through van 't Hoff's analysis directly reflect the specific interactions between the solute and the solvent [33]; finally, to avoid the spurious statistical correlation between enthalpy and entropy described by Krug, Hunter, and Grieger, the thermodynamic analysis is formulated using the harmonic mean temperature (T_{hm}) of the experimental interval as a reference [18,34]:

$$T_{\text{hm}} = \frac{n}{\sum_{i=1}^{n} \frac{1}{T_i}} \tag{1}$$

where n is the number of temperatures evaluated.

Thus, the experimental data on the solubility of TCC are fitted using the modified van't Hoff equation based on T_{hm}:

$$\left[\frac{\partial \ln x_2}{\partial\left(T^{-1} - T_{\text{hm}}^{-1}\right)}\right]_p = -\frac{\Delta_{\text{soln}} H^\circ}{R} \tag{2}$$

$$\ln x_2 = a + m\left(\frac{1}{T} - \frac{1}{T_{\text{hm}}}\right) \tag{3}$$

When evaluating at $T = T_{\text{hm}}$, the term in parentheses cancels out, so that the intercept a and the slope b are statistically uncorrelated (zero covariance between estimators); therefore, the Intercept (a) corresponds to $\ln x_2(T_{\text{hm}})$, and the slope (b) corresponds to $-\frac{\Delta H_{\text{sol}}^\circ}{R}$.

Therefore, the standard Gibbs free energy of the solution evaluated at the harmonic mean temperature T_{hm} is determined directly from the intercept of the fit:

$$\Delta G^{\circ}_{sol} = -RT_{hm}\, a = -RT_{hm} \ln x_2 \quad (4)$$

where, R is the gas constant ($8.314\ J \cdot mol^{-1} \cdot K^{-1}$).

Thus, the standard enthalpy of solution is obtained from the slope b:

$$\Delta H^{\circ}_{sol} = -R \cdot b = -R\left(\frac{\partial \ln x_2}{\partial(1/T - 1/T_{hm})}\right)_P \quad (5)$$

Under the approximation that the specific heat capacity of the solution remains constant within the studied temperature range ($\Delta C^{\circ}_p \approx 0$), ΔH°_{sol} is constant and independent of temperature within that range.

The solution entropy is calculated from the values of $\Delta_{soln}G^{\circ}$, $\Delta_{soln}H^{\circ}$, and T_{hm}:

$$\Delta_{soln}S^{\circ} = (\Delta_{soln}H^{\circ} - \Delta_{soln}G^{\circ})T^{-1}_{hm} \quad (6)$$

Finally, the evaluation of the energy and organizational contributions to Gibbs energy is calculated using Equations (7) and (8)

$$\zeta_H = |\Delta_{soln}H^{\circ}|(|T\Delta_{soln}S^{\circ}| + |\Delta_{soln}H^{\circ}|)^{-1} \quad (7)$$

$$\zeta_{TS} = 1 - \zeta_H \quad (8)$$

Table 3. Thermodynamic functions of the solution process of TTC (2) in some organic solvent at $T_{hm} = 295.21$ K.

Solvent	$\Delta_{soln}G^{\circ}$ (kJ/mol)	$\Delta_{soln}H^{\circ}$ (kJ/mol)	$\Delta_{soln}S^{\circ}$ (J/mol· K)	$T_{hm}\Delta_{soln}S^{\circ}$ (kJ/mol)	ζ_H	ζ_{TS}
N,*N*-dimethylformamide	8.58 ± 0.16	15.01 ± 0.41	21.78 ± 0.09	6.43 ± 0.44	0.636	0.364
methanol	12.36 ± 0.46	27.99 ± 1.57	52.96 ± 0.06	15.63 ± 1.63	0.694	0.306
ethanol	13.04 ± 0.54	31.98 ± 1.98	64.18 ± 0.07	18.95 ± 2.05	0.710	0.290
n-propanol	14.01 ± 0.63	36.04 ± 2.42	74.63 ± 0.07	22.03 ± 2.50	0.720	0.280
i-propanol	15.67 ± 0.79	42.02 ± 3.17	89.28 ± 0.10	26.36 ± 3.27	0.728	0.272
n-butanol	14.97 ± 0.73	40.02 ± 2.92	84.85 ± 0.12	25.05 ± 3.01	0.728	0.272
n-octanol	17.19 ± 0.99	44.99 ± 3.91	94.18 ± 0.11	27.80 ± 4.03	0.724	0.276
1,4-dioxane	15.45 ± 0.32	60.18 ± 1.86	151.50 ± 5.05	44.72 ± 1.88	0.796	0.204
n-hexane	30.30 ± 2.36	30.00 ± 3.50	−1.02 ± 0.03	−0.30 ± 4.23	0.497	0.503
cyclohexane	30.96 ± 2.44	28.95 ± 3.42	−6.82 ± 0.05	−2.01 ± 4.20	0.483	0.517

When analyzing the standard Gibbs free energy of solution ($\Delta_{soln}G^{\circ}$), it is observed that all values are positive over the evaluated interval, ranging from a minimum of 8.58 ± 0.16 kJ/mol for DMF to a maximum of 30.96 ± 2.44 kJ/mol for CHN. Since a decrease in the magnitude of $\Delta_{soln}G^{\circ}$ reflects a direct increase in the solute–solvent thermodynamic affinity (which translates to higher solubility in mole fraction), it is concluded that DMF provides the most favorable molecular environment for the solvation of TTC. Within the homologous series of linear alcohols, the value of $\Delta_{soln}G^{\circ}$ increases with increasing aliphatic chain length, ranging from 12.36 ± 0.46 kJ/mol in MeOH, 13.04 ± 0.54 kJ/mol in EtOH, 14.01 ± 0.63 kJ/mol in *n*-PrOH, and 14.97 ± 0.73 kJ/mol in *n*-BtOH, until reaching 17.19 ± 0.99 kJ/mol in *n*-OcOH. This systematic decrease in affinity is accentuated when there is branching in the aliphatic backbone, as evidenced by the increase in $\Delta_{soln}G^{\circ}$ in *i*-PrOH (15.67 ± 0.79 kJ/mol) compared with its linear isomer *n*-PrOH (14.01 ± 0.63 kJ/mol). DX, on the other hand, exhibits an intermediate affinity ($\Delta_{soln}G^{\circ} = 15.45 \pm 0.32$ kJ/mol), whereas in nonpolar hydrocarbons such as *n*-Hex (30.30 ± 2.36 kJ/mol) and CHN (30.96 ± 2.44 kJ/mol), the high Gibbs energy values reflect a low affinity between the solute and the solvent. Upon analyzing the energy and organizational components, it is observed that the apparent standard enthalpy of solution ($\Delta_{soln}H^{\circ}$) is positive in all cases, indicating an endothermic

dissolution process. Physically, this indicates that the energy released during the subprocess of mixing and the formation of new solute–solvent interactions is less than the endothermic cost required to overcome the cohesive forces of the drug's crystal lattice and to restructure the solvent molecules to form the cavity that accommodates the solute. DMF has the lowest enthalpy value (15.01 ± 0.41 kJ/mol), which may indicate that its specific interactions with TTC compensate for the energy expenditure associated with molecular separation. For linear alcohols, $\Delta_{soln}H^{\circ}$ increases from MeOH (27.99 ± 1.57 kJ/mol) to *n*-OcOH (44.99 ± 3.91 kJ/mol). This increase in energy cost can be attributed to the fact that, as the aliphatic chain of the alcohol grows longer, it becomes more energetically costly to separate the longer, more cohesive aliphatic chains to create the cavity, while at the same time the density of hydroxyl groups capable of releasing energy through solvation decreases. Similarly, i-PrOH exhibits a higher enthalpy requirement (42.02 ± 3.17 kJ/mol) compared with n-PrOH (36.04 ± 2.42 kJ/mol) and *n*-BtOH (40.02 ± 2.92 kJ/mol), confirming that the steric hindrance of its branched structure weakens the exothermic solute–solvent interactions. The maximum value of $\Delta_{soln}H^{\circ}$ is observed for DX (60.18 ± 1.86 kJ/mol), indicating a high cost of disrupting the solvent matrix, whereas n-Hex (30.00 ± 3.50 kJ/mol) and CHX (28.95 ± 3.42 kJ/mol) exhibit intermediate enthalpy values governed almost exclusively by the solute's melting energy and weak dispersion forces.

As for the apparent standard entropy of solution ($\Delta_{soln}S^{\circ}$) and the entropy-energy term ($T_{hm}\Delta_{soln}S^{\circ}$), they are positive in all polar media (DMF, alcohols, and DX), which favors the dissolution process. In DMF, the entropy values are moderate ($\Delta_{soln}S^{\circ} = 21.78 \pm 0.09$ J/mol · K; $T_{hm}\ \Delta_{soln}S^{\circ} = 6.43 \pm 0.044$ kJ/mol), possibly due to the local ordering generated by the specific solvation between the drug and the solvent. As for linear alcohols, the entropy $\Delta_{soln}S^{\circ}$ increases from 52.96 ± 0.06 J/mol · K ($T_{hm}\Delta_{soln}S^{\circ} = 15.63 \pm 1.63$ kJ/mol) in MeOH to 94.18 ± 0.11 J/mol · K ($T_{hm}\Delta_{soln}S^{\circ} = 27.80 \pm 4.03$ kJ/mol) in *n*-OcOH. This increase in entropy gain is closely linked to the increased conformational flexibility and the possible denaturation of the long aliphatic chains upon accommodating the TTC molecule, which generates a greater number of configurational microstates that compensate for the high enthalpic cost of the organic medium. As for DX, the process reaches the maximum entropy value ($\Delta_{soln}S^{\circ} = 151.50 \pm 5.05$ J/mol · K; $T_{hm}\Delta_{soln}S^{\circ} = 44.72 \pm 1.88$ kJ/mol). In contrast, in the nonpolar solvents n-Hex and CHN, the solution entropy becomes negative ($\Delta_{soln}S^{\circ}$ of -1.02 ± 0.03 and -6.82 ± 0.05 J/mol · K, with $T_{hm}\ \Delta_{soln}S^{\circ}$ of -0.30 ± 4.23 and -2.01 ± 4.20 kJ/mol, respectively). In these two hydrocarbons, the process suffers a double thermodynamic penalty (it is endothermic and exhibits an entropy loss due to structural confinement of the solute by the solvent), which conclusively explains the nearly zero affinity of TTC in these media.

Finally, evaluating the relative enthalpy (ζ_H) and entropy (ζ_{TS}). In DMF, for all alcohols and DX, the enthalpic coefficient (ζ_H, ranging from 0.636 in DMF to 0.796 in DX and from 0.694 to 0.728 for the alcohol series) clearly predominates over the entropic coefficient (ζ_{TS}, ranging from 0.204 to 0.364). In general, although entropy is positive, which favors the process, the enthalpy term is the largest contributor to the Gibbs energy, possibly due to the greater energy associated with solute–solvent molecular interactions. In nonpolar solvents, such as *n*-Hex ($\zeta_H = 0.497$, and 0.503 for the entropic coefficient) and CHN ($\zeta_H = 0.483$, and 0.517 for the entropic coefficient), there is a balance, with a slight numerical predominance of the entropic term over the enthalpic term, which may be related to interactions between the solute and the solvent that are energetically lower compared with the dissolution process in other solvents.

3.3. Analysis of the Effect of the Solvent Using the KAT-LSER Model

To quantitatively describe the linear characteristics of Gibbs free energy in the solute–solvent system and elucidate the effect of solvation on the dissolution process at the molecular level, Kamlet, Abboud, and Taft developed the linear solvation energy relationship (LSER) model (also known as the Kamlet–Abboud–Taft (KAT) LSER). This thermodynamic formalism posits that any property of the transfer or dissolution process that depends on free energy is the sum of the endothermic work needed to overcome the solvent's cohesive forces to create a cavity large enough for the solute and the energy change from the specific and non-specific interactions when the solute molecule is incorporated into the liquid environment. This is generally expressed by the following equation [35]:

$$\mathrm{XYZ} = \mathrm{XYZ}_0 + \text{cavity formation energy} + \sum \text{solute–solvent interaction energy} \quad (9)$$

Where XYZ represents the solvent-dependent thermodynamic property, which corresponds to the natural logarithm of solubility in mole fraction ($\ln x$) in phase-equilibrium studies, and XYZ_0 is the reference parameter or intercept of the model in the absence of environmental perturbations [36].

Applying this theoretical expression to the study of solid–liquid equilibrium, incorporating the Kamlet–Taft solvatochromic parameters and Hildebrand's cohesive energy density yields a multiparameter linear expression linking the electronic and structural properties of solvent and solute molecules, as defined by the following equation [22–24]:

$$\ln x = c_0 + c_1\pi^* + c_2\beta + c_3\alpha + c_4\left(\frac{V_s\delta_1^2}{100RT}\right) \quad (10)$$

The first three descriptors (π^*, β and α) quantify the energy contribution of solute–solvent attractive forces. The parameter π^* expresses the dipolarity/polarizability of the selected solvent. This reflects its ability to stabilize solute charges or dipoles through electrostatic and non-specific dispersion forces. The parameter β refers to hydrogen-bond basicity, or the solvent's hydrogen-bond accepting capacity. The parameter α describes hydrogen-bond acidity, or the solvent's hydrogen-bond donating capacity. The fourth term ($V_s\delta_1^2/100RT$) models the energy required for cavity formation as a function of the liquid medium's autocohesiveness. Here, V_s corresponds to the molar volume of the solute; δ_1 represents the Hildebrand solubility parameter of the pure solvent; R is the universal ideal gas constant and T is the absolute temperature of the system. The numerical factor $100RT$ in the denominator makes the energy term dimensionless and scales it appropriately. Multiple linear regression analysis is used to determine the independent term c_0, which represents the intrinsic reference solubility when $\pi^* = \beta = \alpha = \delta_1 = 0$, as well as the susceptibility coefficients c_1, c_2, c_3, and c_4, whose magnitudes and algebraic signs describe the strength and direction of the interactions between the solute and solvents. Specifically, positive values of the coefficients c_1, c_2, or c_3 indicate that an increase in the solvent's dipolarity, polarizability, or hydrogen-bonding capacity thermodynamically favors dissolution. Negative values indicate that these specific or nonspecific interactions are unfavorable for drug solvation. Similarly, a negative c_4 coefficient demonstrates that solubility is inversely correlated with the solvent's self-cohesiveness. This confirms the unfavorable nature of the work required to break the pure liquid's associated structure during cavity formation [23,37].

The analysis of the intermolecular interactions that govern the dissolution process of tetracycline (TTC) at 298.15 K in pure organic systems using the Kamlet–Abboud–Taft linear solvation energy relationship (KAT-LSER) model is described by the equation (see Table 4):

$$\ln(x_2) = -11.5269 + 1.4617\alpha + 0.2093\beta + 9.7953\pi^* - 1.0216C \quad (11)$$

Table 4. Coefficient and statistical values for Equation (11).

Variable	Coef	Std Err	t	$p > \|t\|$	[0.025	0.975]
c_0	−11.5269	0.992	−11.624	0.000	−14.076	−8.978
c_1	1.4617	1.957	0.747	0.489	−3.568	6.492
c_2	0.2093	2.501	0.084	0.937	−6.219	6.637
c_3	9.7953	3.025	3.238	0.023	2.020	17.571
c_4	−1.0216	4.046	−0.253	0.811	−11.422	9.378

Standard Errors assume that the covariance matrix of the errors is correctly specified.

The equation was calculated based on the experimental solubility values of TTC at 298.15 K in 10 organic solvents (see Table 1) and the respective values of the Hildebrand solubility parameter and the solvatochromic parameters of each of the pure solvents (see Table 5).

Table 5. Hildebrand solubility parameters (δ_1) and solvatochromic parameters (δ, α, β, π^*) or the selected solvents [31,38].

Solvent	δ/MPa$^{1/2}$	α	β	π^*
N,*N*-dimethylformamide	24.80	0.88	0.00	0.69
methanol	29.7	0.60	0.98	0.66
ethanol	26.1	0.54	0.86	0.75
n-propanol	24.9	0.52	0.84	0.90
i-propanol	23.4	0.48	0.76	0.84
n-butanol	23.7	0.47	0.84	0.84
n-octanol	21.1	0.40	0.77	0.81
1,4-dioxane	20.07	0.55	0.00	0.37
n-hexane	15.0	-0.11	0.00	0.00
cyclohexane	16.08	0.00	0.00	0.00

The term C ($V_s\delta_1^2/100RT$) quantifies the energy requirement for cavity formation as a function of the molar volume of the solute and the square of the Hildebrand solubility parameter of the solvent (δ_1^2) [24,37].

Results from a statistical analysis of the model using multiple linear regression with ordinary least squares (OLS) and based on data from 10 pure organic solvents show mathematical robustness. This robustness is supported by a multiple correlation coefficient of 0.9932 and coefficients of determination (see Table 6). These coefficients indicate that the model explains 98.64% of the total variance ($R^2 = 0.986$) and 97.55% of the experimental variance in solubility, adjusted for degrees of freedom ($R^2_{adj} = 0.976$). The model's overall validity is confirmed by a low residual sum of squares (RSS = 1.1183) and a significant F-statistic of 90.77 ($p = 7.4534 \times 10^{-5}$).

The diagnostic statistics (see Table 6) also validate the model's parametric assumptions. The Durbin–Watson statistic (2.062, close to the ideal value of 2.0) shows that the residuals are independent and free of autocorrelation. The omnibus (2.422, $p = 0.298$) and Jarque-Bera (0.455, $p = 0.797$) normality tests, together with moderate skewness (−0.470) and kurtosis (3.457, close to the normal value of 3.0), show that the errors follow a normal distribution. The condition number (57.4) indicates moderate and acceptable collinearity among the organic descriptors.

Table 6. Statistical summary of the ordinary least squares (OLS) regression and diagnostic statistics for the residuals of the KAT-LSER model for tetracycline.

Parameter	Value	Parameter	Value
Dependent variable	$\ln x_2$	R^2	0.986
Model	OLS	Adjusted R^2	0.976
Method	Least squares	F-statistic	90.77
		Prob (F-statistic)	7.45×10^{-5}
Statistician	Value	Statistician	Value
Omnibus	2.422	Durbin–Watson	2.062
Prob (Omnibus)	0.298	Jarque–Bera (JB)	0.455
Skewness	−0.470	Prob (JB)	0.797
Kurtosis	3.457	Condition No.	57.4

By analyzing the magnitude, sign, and statistical significance of each regression coefficient, we can elucidate the molecular mechanisms that promote or inhibit drug solvation in organic media (see Table 6). The intercept is statistically significant ($c_0 = -11.5269$, $t = -11.624$, $p < 0.001$), and its negative value reflects the energy barrier associated with strong solute–solute interactions within the TTC crystal lattice that must be overcome for incorporation into the liquid phase. Upon analyzing the dissolution-favoring terms, it was observed that the three solvatochromic parameters had positive signs: polarizability/dipolarity (π^* with $c_3 = 9.7953$, $t = 3.238$, and $p = 0.023$), hydrogen-bond-donating acidity (α with $c_1 = 1.4617$, $t = 0.747$, and $p = 0.489$), and hydrogen-bond-accepting basicity (β with $c_2 = 0.2093$, $t = 0.084$, and $p = 0.937$). The π^* term is the only statistically significant explanatory variable at the 95% confidence level, accounting for 76.04% of the total variance. This shows that, in organic solvents, TTC's solvation is primarily governed by dipole–dipole interactions, induced dipole–dipole interactions, and forces acting on the drug's polar centers and electron-rich π-conjugated tetracyclic system. Meanwhile, the α term represents the second-largest relative contribution (17.27%), and the β term contributes minimally (1.93%). Although both terms have positive signs, consistent with the amphiprotic stabilization of TTC's functional groups (carbonyl oxygens, amide group, dimethylamino group, and multiple hydroxyl groups), their $p > 0.05$ values indicate that the variability of hydrogen-bond interactions within this organic subset is statistically subsumed by the strong predictive power of the π^* descriptor.

In contrast, the term corresponding to cavity formation (C, with $c_4 = -1.0216$, $t = -0.253$, and $p = 0.811$) is the only one with a negative sign. This confirms the endothermic nature associated with overcoming the solvent's cohesive energy density (δ_1^2) and accommodating the bulky TTC molecule ($V = 216.3$ cm^3/mol).

Finally, comparing the logarithm of the experimental solubility ($\ln x_{exp}$) to the calculated solubility ($\ln x_{calc}$) shows the KAT-LSER model's ability to predict solubility across more than three orders of magnitude in mole fraction when fitted for ten pure solvents. The alcohol series and the protic and aprotic polar solvents fall within the tolerance range of ±0.5 logarithmic units relative to the ideal correlation line ($y = x$), which reduces relative errors in mole fraction (see Table 7 and Figure 6a).

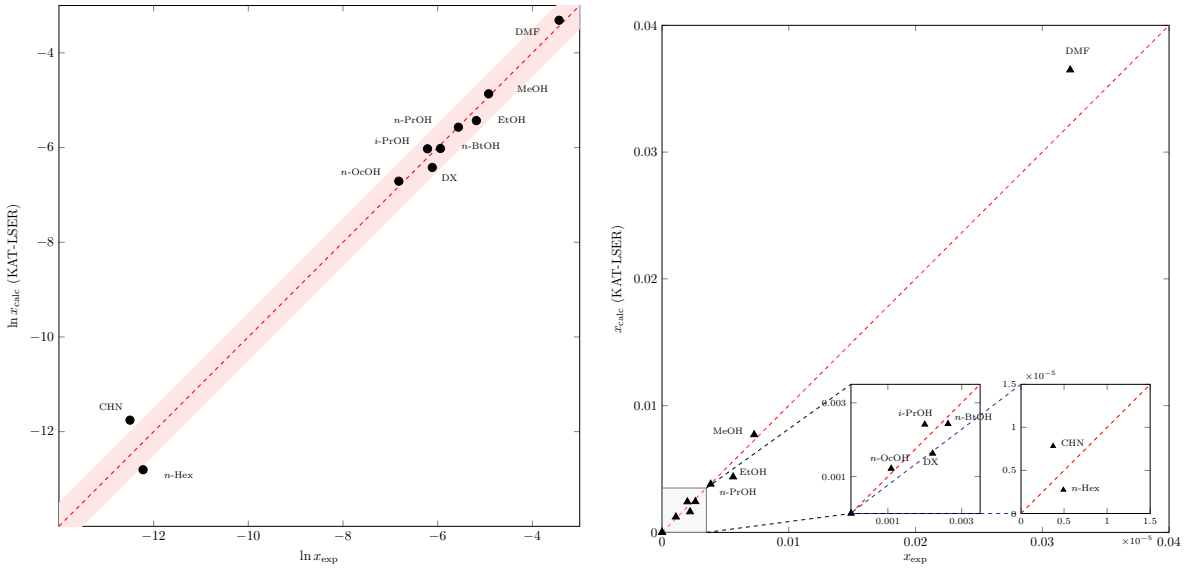
Specifically, outstanding accuracy is achieved for *n*-PrOH (residue of 0.0075; relative error of 0.75%), followed by MeOH (residue of −0.0586; error of 6.03%), *n*-BtOH (residue of 0.0794; error of 7.63%), *n*-OcOH (residue of −0.1110; error of 11.74%), DMF (residue of −0.1248; error of 13.3%), *i*-PrOH (residue of −0.1881; error of 20.69%), and EtOH (residue of 0.2474; error of 21.92% error), and DX (0.3072 residue; 26.45% error). The only discrepancies greater than half a logarithmic unit are limited to the nonpolar hydrocarbons *n*-Hex and CHN. The residue of *n*-Hex is 0.5827 with a relative error of 44.16%, and the residue of CHN

is −0.7417 with a relative error of 109.96%. The total absence of dipole moment and specific interactions results in extremely low solubilities (on the order of 10^{-6}), which amplifies any numerical variation when converting from the logarithmic scale to direct mole fraction in percentage terms.

Figure 6b shows the results of the KAT-LSER solvation model on a linear scale. Similar to the logarithmic scale, the linear scale shows good agreement between the experimental and calculated data, except for DX and CHN, for which the relative error exceeds 44%.

Table 7. Solubility of TTC in different solvents calculated using the KAT-LSER model.

Solvent	$\ln(x_{Exp})$	$\ln(x_{Calc})$	Residual [ln]	x_{Exp}	x_{Calc}	Relative Error (%)
N,*N*-dimethylformamide	−3.4358	−3.3109	−0.1248	3.2200×10^{-2}	3.6482×10^{-2}	13.30%
methanol	−4.9240	−4.8654	−0.0586	7.2700×10^{-3}	7.7085×10^{-3}	6.03%
ethanol	−5.1832	−5.4306	0.2474	5.6100×10^{-3}	4.3804×10^{-3}	21.92%
n-propanol	−5.5623	−5.5698	0.0075	3.8400×10^{-3}	3.8112×10^{-3}	0.75%
i-propanol	−6.2146	−6.0266	−0.1881	2.0000×10^{-3}	2.4138×10^{-3}	20.69%
n-butanol	−5.9408	−6.0201	0.0794	2.6300×10^{-3}	2.4293×10^{-3}	7.63%
n-octanol	−6.8216	−6.7106	−0.1110	1.0900×10^{-3}	1.2179×10^{-3}	11.74%
1,4-dioxane	−6.1140	−6.4212	0.3072	2.2117×10^{-3}	1.6268×10^{-3}	26.45%
n-hexane	−12.2222	−12.8049	0.5827	4.9200×10^{-6}	2.7472×10^{-6}	44.16%
cyclohexane	−12.4991	−11.7574	−0.7417	3.7300×10^{-6}	7.8314×10^{-6}	109.96%



(**a**) (**b**)

Figure 6. Correlation between experimental solubility and solubility calculated using the KAT-LSER solvation model in 10 pure solvents. The red dashed line indicates the ideal correlation ($y = x$), and the shaded area represents a tolerance margin of ±0.5 logarithmic units in the graph at T_{hm} = 295.21 K. (**a**) Logarithmic scale (**b**) Linear scale.

4. Conclusions

The equilibrium solubility of tetracycline in ten pure organic solvents increases systematically with temperature between 278.15 K and 313.15 K, reaching its maximum value in *N*,*N*-dimethylformamide and its minimum in cyclohexane, while it decreases in alcohols as the aliphatic chain becomes longer or more branched. FTIR analysis confirmed that the drug retains its chemical integrity and original crystalline structure without exhibiting polymorphism. According to the Gibbs–van't Hoff–Krug model, dissolution is endothermic

($\Delta_{soln}H^\circ > 0$) and is favored primarily by enthalpy in polar media. Finally, the KAT-LSER model demonstrated that solvation is governed primarily by the dipolarity/polarizability (π^*) of the solvent.

Supplementary Materials: The following supporting information can be downloaded at: https://www.mdpi.com/article/10.3390/liquids6040035/s1, A detailed description of the experimental methodology is provided. Table S1: Source and purity of the compounds used in this research.

Author Contributions: Conceptualization, J.K.C.-C., F.M. and D.R.D.; methodology, K.M.G.-D., F.E.A.-L. and D.R.D.; software, K.M.G.-D., F.E.A.-L., L.D.O.-M. and D.R.D.; validation, F.M. and D.R.D.; formal analysis, K.M.G.-D., F.E.A.-L. and D.R.D.; investigation, K.M.G.-D., F.E.A.-L., J.K.C.-C., F.M. and D.R.D.; resources, D.R.D.; data curation, F.M.; writing—original draft preparation, L.D.O.-M. and D.R.D.; writing—review and editing, F.M. and D.R.D.; visualization, F.M.; supervision, F.M. and D.R.D.; project administration, D.R.D.; funding acquisition, D.R.D. All authors have read and agreed to the published version of the manuscript.

Funding: This research was funded by the Universidad Cooperativa de Colombia grant number INV3883.

Institutional Review Board Statement: Not applicable.

Informed Consent Statement: Not applicable.

Data Availability Statement: Data are contained within the article.

Acknowledgments: We thank the National Directorate of Research and National Committee for Research Development of the Universidad Cooperativa de Colombia for the financial support of the project "Análisis termodinámico y modelamiento mediante aprendizaje automático de la solubilidad de algunos antimicrobianos en sistemas acuosos poliméricos." with code INV3883. We also thank the Universidad Cooperativa de Colombia, Sede Neiva, for facilitating the use of their laboratories and equipment.

Conflicts of Interest: The authors declare no conflicts of interest.

Abbreviations

The following abbreviations are used in this manuscript:

a	Intercept of the van't Hoff–Krug equation
aa-tRNA	Aminoacyl-transfer ribonucleic acid
AMR	Antimicrobial resistance
ARGs	Antibiotic resistance genes
C	Cavity formation energy term (and Kelvin for temperature units)
c_0	Reference intercept of the KAT-LSER model
c_1, c_2, c_3, c_4	Susceptibility coefficients of the KAT-LSER model
CHN	Cyclohexane
DMF	*N*,*N*-Dimethylformamide
DX	1,4-Dioxane
EtOH	Ethanol
FTIR	Fourier-transform infrared spectroscopy
i-PrOH	*i*-Propanol (Isopropanol)
IR	Infrared spectroscopy
JB	Jarque–Bera normality statistic
KAT-LSER	Kamlet–Abboud–Taft Linear Solvation Energy Relationship
LSER	Linear Solvation Energy Relationship
m	Slope of the van't Hoff–Krug equation
MeOH	Methanol
n-BtOH	*n*-Butanol
n-Hex	*n*-Hexane
n-OcOH	*n*-Octanol
n-PrOH	*n*-Propanol

OLS	Ordinary least squares
p	Experimental pressure
R	Universal gas constant (8.314 J/mol · K)
R^2	Coefficient of determination
R^2_{adj}	Adjusted coefficient of determination
RSS	Residual sum of squares
T	Study temperature
T_{hm}	Harmonic mean temperature (295.21 K)
TTC	Tetracycline
UV/Vis	Ultraviolet–visible spectrophotometry
V_s	Molar volume of the solute
WWTPs	Wastewater treatment plants
x_2	Mole fraction solubility of tetracycline
x_{exp}, x_{calc}	Experimental and calculated mole fraction solubility
α	Kamlet–Taft hydrogen-bond donating acidity
β	Kamlet–Taft hydrogen-bond accepting basicity
π^*	Kamlet–Taft dipolarity/polarizability parameter
δ_1, δ_2	Hildebrand solubility parameter of the solvent (**1**) and solute (**2**)
ΔU	Cohesive energy
$\Delta_{soln}G^\circ$	Apparent standard Gibbs energy of solution
$\Delta_{soln}H^\circ$	Apparent standard enthalpy of solution
$\Delta_{soln}S^\circ$	Apparent standard entropy of solution
ζ_H	Relative enthalpic contribution to the standard Gibbs energy of solution
ζ_{TS}	Relative entropic contribution to the standard Gibbs energy of solution

References

1. Li, J.; Qin, Y.; Zhao, C.; Zhang, Z.; Zhou, Z. Tetracycline antibiotics: Potential anticancer drugs. *Eur. J. Pharmacol.* **2023**, *956*, 175949. [CrossRef] [PubMed]
2. Mohamadi, B.; Akbari, N.; Miri, P.; Shokri, S.; Aghebat-Bekheir, S.; Sadighara, P. Amount, sources, and methods of identifying tetracycline in eggs: A systematic review. *Meas. Food* **2026**, *23*, 100317. [CrossRef]
3. V, N.; Singh, C.K.; Kumar, N.; Rawat, S.S.; Sodhi, K.K. Rethinking tetracycline in the Anthropocene: From miracle drugs to emerging environmental contaminants. *Sci. Total Environ.* **2026**, *1012*, 181265. [CrossRef]
4. Daghrir, R.; Drogui, P. Tetracycline antibiotics in the environment: A review. *Environ. Chem. Lett.* **2013**, *11*, 209–227. [CrossRef]
5. Cui, C.Y.; Chen, Q.; He, Q.; Chen, C.; Zhang, R.M.; Feng, Y.; Sun, J. Transferability of tigecycline resistance: Characterization of the expanding Tet(X) family. *WIREs Mech. Dis.* **2022**, *14*, e1538. [CrossRef] [PubMed]
6. Fang, L.X.; Chen, C.; Cui, C.Y.; Li, X.P.; Zhang, Y.; Liao, X.P.; Sun, J.; Liu, Y.H. Emerging High-Level Tigecycline Resistance: Novel Tetracycline Destructases Spread via the Mobile Tet(X). *BioEssays* **2020**, *42*, 2000014. [CrossRef] [PubMed]
7. Rusu, A.; Buta, E.L. The Development of Third-Generation Tetracycline Antibiotics and New Perspectives. *Pharmaceutics* **2021**, *13*, 2085. [CrossRef]
8. Jia, Y.; Luo, S.; Wang, X.; Li, W.; Li, B.; Zhang, D. Novel insight into diversity of active tetracycline-resistant bacteria and genes in sludge by in situ microcapsule-entrapped cultivation. *Bioresour. Technol.* **2027**, *464*, 135849. [CrossRef]
9. Murray, C.J.L.; Ikuta, K.S.; Sharara, F.; Swetschinski, L.; Robles Aguilar, G.; Gray, A.; Han, C.; Bisignano, C.; Rao, P.; Wool, E.; et al. Global burden of bacterial antimicrobial resistance in 2019: A systematic analysis. *Lancet* **2022**, *399*, 629–655. Correction in *Lancet* **2022**, *400*, 1102. [CrossRef] [PubMed]
10. NORMAN List of Emerging Substances. Available online: https://www.norman-network.net/?q=node/81 (accessed on 23 September 2026).
11. Sun, J.; He, Z. Enhanced tetracycline removal through integrated adsorption, biodegradation, and chemical degradation in H_2O_2 assisted VFAs-producing anaerobic digestion. *J. Environ. Chem. Eng.* **2026**, *14*, 123681. [CrossRef]
12. Zeng, J.; Wei, L.; Liu, Z.; Liu, Y.; Zhang, H.; Liu, W. MnOx-biochar substrates improve tetracycline removal and potentially restrain antibiotic resistance gene accumulation in constructed wetlands. *Int. Biodeterior. Biodegrad.* **2027**, *216*, 106478. [CrossRef]
13. Zhang, G.; Zhang, D.; Li, W. Assessment of bioavailability of microplastic-sorbed tetracycline to bacteria for activation of antibiotic resistance genes in water environments. *Aquat. Toxicol.* **2026**, *293*, 107769. [CrossRef]
14. Delgado, D.R.; Castro-Camacho, J.K.; Ortiz, C.P.; Caviedes-Rubio, D.I.; Martinez, F. Dissolution Thermodynamics of the Solubility of Sulfamethazine in (Acetonitrile + 1-Propanol) Mixtures. *Pharmaceuticals* **2024**, *17*, 1594. [CrossRef] [PubMed]
15. Amézqueta, S.; Subirats, X.; Fuguet, E.; Rosés, M.; Ràfols, C. Octanol-Water Partition Constant. In *Liquid-Phase Extraction*; Poole, C.F., Ed.; Handbooks in Separation Science; Elsevier: Amsterdam, The Netherlands, 2020; pp. 183–208. [CrossRef]
16. Pade, V.; Stavchansky, S. Link between drug absorption solubility and permeability measurements in Caco-2 cells. *J. Pharm. Sci.* **1998**, *87*, 1604–1607. [CrossRef]

17. Sinko, P. *Martin's Physical Pharmacy and Pharmaceutical Sciences*; Wolters Kluwer Health: Waltham, MA, USA, 2023.
18. Krug, R.R.; Hunter, W.G.; Grieger, R.A. Enthalpy-entropy compensation. 2. Separation of the chemical from the statistical effect. *J. Phys. Chem.* **1976**, *80*, 2341–2351. [CrossRef]
19. Prausnitz, J.; Lichtenthaler, R.; de Azevedo, E. *Molecular Thermodynamics of Fluid-Phase Equilibria*; Pearson Education: London, UK, 1998.
20. Martinez Romero, P.N.; Cerquera, N.E.; Cardenas-Torres, R.E.; Martinez, F.; Delgado, D.R. Thermodynamic Insights into Isoniazid Solubility in PEG 300 + Water Mixtures. *Liquids* **2026**, *6*, 23. [CrossRef]
21. Kontogeorgis, G.; Folas, G. *Thermodynamic Models for Industrial Applications: From Classical and Advanced Mixing Rules to Association Theories*; Wiley: Hoboken, NJ, USA, 2009.
22. Taft, R.W.; Abboud, J.L.M.; Kamlet, M.J.; Abraham, M.H. Linear solvation energy relations. *J. Solut. Chem.* **1985**, *14*, 153–186. [CrossRef]
23. Kamlet, M.J.; Doherty, R.M.; Abboud, J.L.M.; Abraham, M.H.; Taft, R.W. Linear Solvation Energy Relationships: 36. Molecular Properties Governing Solubilities of Organic Nonelectrolytes In Water. *J. Pharm. Sci.* **1986**, *75*, 338–349. [CrossRef] [PubMed]
24. Kamlet, M.J.; Doherty, R.; Abboud, J.L.M.; Abraham, M.K.; Taft, R.W. Solubility: A new look. *Chemtech* **1986**, *16*, 566–576.
25. Higuchi, T.; Connors, K.A. Phase-solubility techniques. *Adv. Anal. Chem. Instrum.* **1965**, *4*, 117–212. [CrossRef]
26. Cacço, A.I.; Varanda, F.; Pratas de Melo, M.J.; Dias, A.M.A.; Dohrn, R.; Marrucho, I.M. Solubility of Antibiotics in Different Solvents. Part II. Non-Hydrochloride Forms of Tetracycline and Ciprofloxacin. *Ind. Eng. Chem. Res.* **2008**, *47*, 8083–8089. [CrossRef]
27. Graff, C. Expressing relative differences (in percent) by the difference of natural logarithms. *J. Math. Psychol.* **2014**, *60*, 82–85. [CrossRef]
28. Johari, G.; Shanker, R.M. On the solubility advantage of a pharmaceutical's glassy state over the crystal state, and of its crystal polymorphs. *Thermochim. Acta* **2014**, *598*, 16–27. [CrossRef]
29. Jouyban, A. Review of the cosolvency models for predicting solubility of drugs in water-cosolvent mixtures. *J. Pharm. Pharm. Sci.* **2008**, *11*, 32–58. [CrossRef] [PubMed]
30. Vertzoni, M.; Alsenz, J.; Augustijns, P.; Bauer-Brandl, A.; Bergström, C.; Brouwers, J.; Müllerz, A.; Perlovich, G.; Saal, C.; Sugano, K.; et al. UNGAP best practice for improving solubility data quality of orally administered drugs. *Eur. J. Pharm. Sci.* **2022**, *168*, 106043. [CrossRef] [PubMed]
31. Barton, A. *CRC Handbook of Solubility Parameters and Other Cohesion Parameters*, 2nd ed.; Taylor & Francis: Abingdon, UK, 1991.
32. Yong-Cheng, N. Interpretation of Mass Spectra. In *Interpretation of Organic Spectra*; John Wiley & Sons, Ltd.: Hoboken, NJ, USA, 2011; Chapter 4, pp. 87–127. [CrossRef]
33. Connors, K.A. *Thermodynamics of Pharmaceutical Systems: An Introduction for Students of Pharmacy*; John Wiley & Sons Ltd.: Hoboken, NJ, USA, 2002.
34. Tovar-Amézquita, J.; Rincón-Guio, C.; Torres-Suarez, F.E.; Florez, M.M.; Ortiz, C.P.; Martinez, F.; Delgado, D.R. Thermodynamic Assessment of the Pyrazinamide Dissolution Process in Some Organic Solvents. *Molecules* **2024**, *29*, 5089. [CrossRef] [PubMed]
35. Panayiotou, C.; Zuburtikudis, I.; Abu Khalifeh, H.; Hatzimanikatis, V. Linear Solvation–Energy Relationships (LSER) and Equation-of-State Thermodynamics: On the Extraction of Thermodynamic Information from the LSER Database. *Liquids* **2023**, *3*, 66–89. [CrossRef]
36. Ben-Naim, A.Y. *Solvation Thermodynamics*; Springer Science & Business Media: Berlin/Heidelberg, Germany, 2013.
37. Kamlet, M.J.; Abboud, J.L.M.; Taft, R.W. An Examination of Linear Solvation Energy Relationships. In *Progress in Physical Organic Chemistry*; John Wiley & Sons, Ltd.: Hoboken, NJ, USA, 1981; pp. 485–630. [CrossRef]
38. Marcus, Y. *The Properties of Solvents*; John Wiley & Sons Ltd.: New York, NY, USA, 1998.

Disclaimer/Publisher's Note: The statements, opinions and data contained in all publications are solely those of the individual author(s) and contributor(s) and not of MDPI and/or the editor(s). MDPI and/or the editor(s) disclaim responsibility for any injury to people or property resulting from any ideas, methods, instructions or products referred to in the content.